Validation of neutron emission profiles in MAST with a collimated neutron monitor

S. Sangaroon, M. Cecconello, S. Conroy, M. Weiszflog, M. Turnyanskiy et al.

Related Articles

Compact steady-state and high-flux Falcon ion source for tests of plasma-facing materials
Rev. Sci. Instrum. 83, 083501 (2012)

Prospects for the Thomson scattering system on NSTX-Upgrade
Rev. Sci. Instrum. 83, 10D532 (2012)

Swinging reciprocating Mach probes for the high field side scrape-off layer in DIII-D
Rev. Sci. Instrum. 83, 10D723 (2012)

Bragg x-ray survey spectrometer for ITER
Rev. Sci. Instrum. 83, 10E126 (2012)

Neutron field parameter measurements on the JET tokamak by means of super-heated fluid detectors
Rev. Sci. Instrum. 83, 10E124 (2012)

Additional information on Rev. Sci. Instrum.

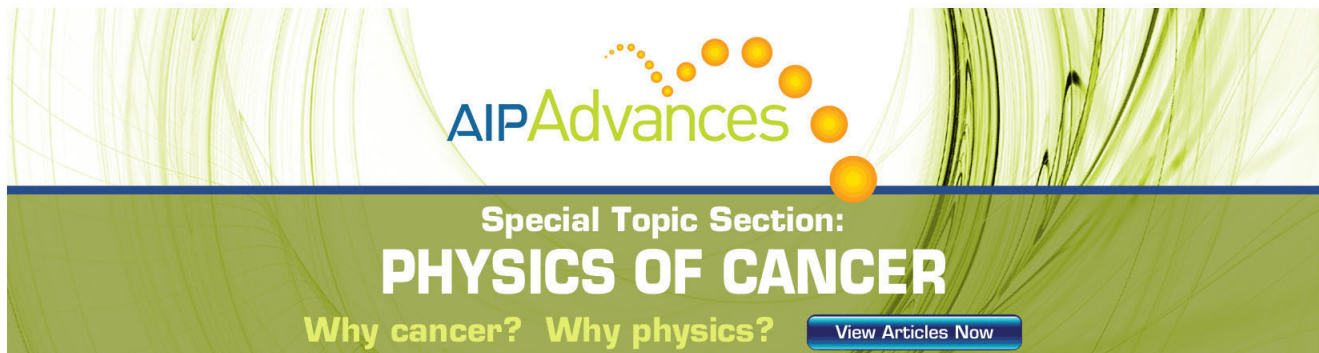Journal Homepage: http://rsi.aip.org

Journal Information: http://rsi.aip.org/about/about_the_journal

Top downloads: http://rsi.aip.org/features/most_downloaded

Information for Authors: http://rsi.aip.org/authors

Validation of neutron emission profiles in MAST with a collimated neutron monitor[a)]

S. Sangaroon,[1,b)] M. Cecconello,[1] S. Conroy,[1] M. Weiszflog,[1] M. Turnyanskiy,[2]
I. Wodniak,[1] and G. Ericsson[1]
[1]*Department of Physics and Astronomy, Uppsala University, EURATOM-VR Association, Uppsala, Sweden*
[2]*EURATOM/CCFE Fusion Association, Culham Science Centre, Abingdon, United Kingdom*

A neutron camera with liquid scintillator detectors is used in MAST to measure the neutron emissivity from $D(d,n)^3$He reactions along collimated lines of sight. In this work, the measured recoil proton pulse height spectra generated in the detectors by the incident neutrons is modelled taking into account the energy spectrum of the generated neutrons, their spatial distribution and transport to the detectors as well as the detector's response function. The contribution of scattered neutrons to the pulse height spectrum is also modelled. Good agreement is found between the experimental data and the simulations. Examples are given showing the sensitivity of the recoil proton pulse height spectra to different observation angles with respect the neutral beam injection and the plasma rotation direction. [http://dx.doi.org/10.1063/1.4732059]

I. INTRODUCTION

The mega amp spherical tokamak (MAST) is a medium size device with a poloidal cross session and plasma current comparable to DIII-D and ASDEX Upgrade. MAST is equipped with two neutral beam injectors (NBIs) which can deliver up to 5 MW of additional heating. Neutrons are produced mainly when deuterons are injected in a deuterium plasmas via beam-thermal and beam-beam $D(d,n)^3$He reactions. The neutron emission can be used to diagnose the interplay of MHD instabilities and fast particles and, on MAST, it is measured by a ^{235}U fission chamber (FC) and by a neutron camera (NC).[1] While the FC measures the global neutron yield rate, the NC measures the neutron emissivity along collimated lines of sight (LoS). The NC consists of two equatorial and two diagonal lines of sight whose position relative to the plasma can be changed from pulse to pulse by moving the NC on a rail. The impact parameter p can therefore be varied from 0.2 m (edge of the central column) to 1.2 m (outboard plasma region). The detectors are made of a NE-213 type liquid scintillator. The active area of each detector is 10 cm^2; the thickness is 1.5 cm. The scintillators are coupled to photomultiplier tubes (PMTs) via a short light guide. The detectors are shielded from uncollimated neutrons by a 1 m thick polyethylene shield which also provides the collimated views. Each detector is equipped with a ^{22}Na gamma source used for calibration purposes. A 5 kHz light emitting diode (LED) provides a square light pulse of approximately constant amplitude which is fed via an optic fiber bundle to all four scintillators and is used for monitoring the stability of the PMTs. The PMT linearity is mainly affected by the high total count rates; the effect of stray magnetic fields is strongly reduced thanks to a double soft iron box surrounding the detectors. The individual pulses for each incident neutron or gamma ray are acquired with a 14 bit resolution, 250 MS/s sampling frequency analog-to-digital converter (ADC). Pulse shape analysis, gamma/neutron discrimination, pulse height spectrum analysis, and count rate calculations are done on the digitized stored data.

This work focuses on the characterization of the detectors response to direct and scattered neutrons based on the comparison of measured and simulated proton recoil pulse height spectra (PHS) and neutron emissivity profiles.

II. DATA ANALYSIS

The study here presented is based on measurements performed in MAST plasmas with 3.5 MW of NBI power (Fig. 1(a)). The maximum neutron yield rate measured by the FC is about 1.20×10^{14} s^{-1} (Fig. 1(c)). The total (neutrons and gammas) count rate measured by the NC is as high as 1.20×10^6 s^{-1} as shown in Fig. 1(d). At such high count rates, the PMT response becomes nonlinear as it can be seen in Fig. 1(e) (red curve) where the LED pulses total charge is plotted versus time. This non-linearity affects the proton recoil PHS and therefore must be corrected. The correction (referred to also as compensation) is achieved multiplying the raw data by the factor $Q_{LED(ref)}/\langle Q_{LED(i)}\rangle$ where $Q_{LED(ref)}$ is the average total charge in the LED pulses measured for $t \gg t_{\text{pulse}}$ and $\langle Q_{LED(i)}\rangle$ is the running average of the total charge over 100 LED pulses. This insures that the compensation factor depends only on the PMT gain variations and not on the LED's amplitude variation from one LED pulse to the other. The compensated LED pulses are shown in Fig. 1(e) (black curve). This method allows also for the compensation of any change in the PMT gain due to the residual stray magnetic fields. Standard pulse shape discrimination methods are used to separate neutron and gamma pulses. For each recorded pulse, the charge deposited in the detector in a "short" and "long" time
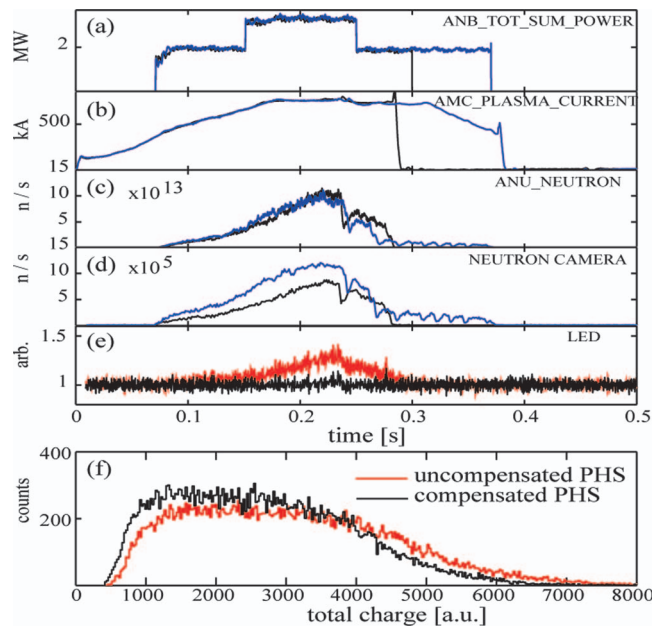

FIG. 1. Time traces for MAST pulses 27047 (black) and 27050 (blue): (a) NBI, (b) plasma current Ip, (c) neutron yield as measured by the FC and (d) total count rates measured by NC, respectively. Panel (e) shows the effect of high count rate on the LED total charge (in red) and the effect of gain compensation (in black) for pulse 27047. Panel (f) shows the uncompensated and compensated recoil proton PHS.

interval is calculated. The short time interval provides a "fast" charge Q_{fast}; the long time interval provides a "slow" charge Q_{slow}. A 2D histogram of $(Q_{slow} - Q_{fast})/Q_{slow}$ versus Q_{slow} results in two well separated clouds of data points, one for neutrons and one for gamma rays which can be easily separated. The importance of a correct PMT compensation on the recoil proton PHS can be seen in Fig. 1(f) where compensated and uncompensated PHS are compared. The compensated recoil proton PHS is used in this work for comparison with the simulated PHS. The simulation of the PHS requires the knowledge of the neutron energy spectrum incident on each detector, of its response function and energy resolution. TRANSP modelling is used to determine the spatial distribution of the neutron source for a given plasma scenario. The neutron energy spectrum is then modelled at different position in the plasma. This neutron source is then used in Monte Carlo N-Particles (MCNP) transport code, together with a proper model of the geometry and material composition of the main components of MAST and of the neutron camera, to calculate the neutron energy spectrum per MAST neutron $\Gamma(E_n)$ reaching the detectors in each collimator (Fig. 2(a)). Finally, the neutron energy spectrum at each detector is used to simulate the detector response using the Monte Carlo code NRESP.[2] The detector response function is then convoluted with the experimentally measured energy resolution function.[3] The detector's response function matrix, that is the recoil proton PHS corresponding to the incident neutrons, was calculated assuming mono-energetic neutrons with energies E_n in the range 0.2–5.0 MeV in steps of 50 keV. The energy resolution function was measured for each detector using the Compton edge of the PHS of gamma rays of different energies as described in Ref. 3. The response function matrix folded with the detector resolution, $R(E_p, E_n)$, corrected for the presence of a trigger-
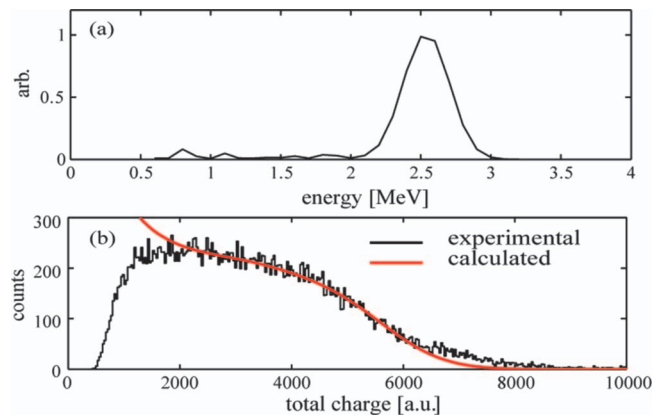

FIG. 2. (a) D-D neutron spectrum for impact parameter 0.87 m. (b) Comparison between the experimental proton recoil PHS for pulse 28276 and the simulation.

ing threshold in the ADC, which is equivalent to a minimum detectable energy E_{TH}, weighted for the neutron energy spectrum at the detector and summed over all incident neutron energies:

$$\text{PHS}(E_p) = A \sum_i R(E_p, E_{n,i}) \Gamma(E_n)$$

provides the simulated PHS where A is the normalization parameter. Figure 2(b) shows the comparison between the experimentally measured (R) and the simulated (S) recoil proton PHS. The χ^2, defined as $\chi^2 = S_i(R_i - S_i)^2/(R_i + S_i)$ where R_i and S_i are the number of events in each bin for the two sets of data, is approximately 1.11. A sensitivity study of the simulated PHS as a function of the bulk ion toroidal velocity and temperature and of the detector energy resolution function has been carried out. As it can be expected, the simulated PHS depends on the plasma rotation: Fig. 3(a) shows the effect of a 50 keV energy shift in the neutron spectrum due to different rotation velocities: the energy shifts with respect to the zero rotation velocity spectrum (in red) are indicated in green and blue for the upward and downward shift, respectively. Figure 3(b) shows the effect of changes in the bulk ions temperature which affects the width of neutron spectrum. The blue and green curves refer to full width at half maximum of 300 keV and 450 keV, respectively. Figure 3(c) shows the impact of different energy resolutions on the simulated PHS: from 25.01% at 2.45 MeV in term of recoil
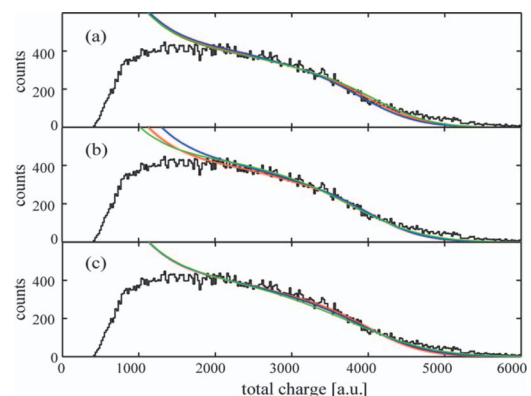

FIG. 3. The sensibility of PHS due to plasma rotation (a), bulk plasma temperature (b), and detector resolution function (c).
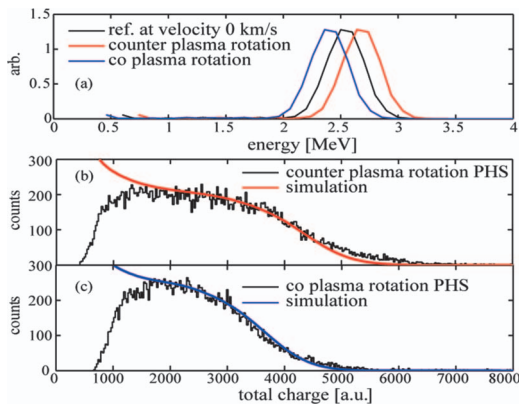
FIG. 4. Panel (a): calculated neutron spectrum from MCNP for counter (red) and co-LoS (blue) with respect to the plasma rotation. Panel (b) comparison between measured and modelled PHS for counter and co-plasma rotation (c).

proton energy (red) to 30.28% (blue) and 37.97% (green). Figure 4 shows the measured PHS when observing the plasma with an impact parameter of 0.64 m counter (panel (b)) and co-plasma (panel (c)) the bulk plasma rotation. As it can be clearly seen the recoil proton PHS are very dependent on the direction of observation with respect to the plasma rotation. In order to simulate the measured PHS, the zero rotation velocity PHS (black curve in Fig. 4(a)) has been up-shifted in energy (red curve in Fig. 4(a)) until the simulated PHS matched the measured one (Fig. 4(b)). The same energy shift (140 keV) was then used to shift down the zero toroidal velocity energy spectrum resulting also in a good match to the experimental measurements: the fit provides $\chi^2 = 0.72$ for the up-shifted spectrum and $\chi^2 = 1.31$ for the down shifted one.

III. SCATTERED NEUTRONS CONTRIBUTION

The back-scattered and in-scattered neutrons contribution to the neutrons energy spectrum depends on the impact parameter of the LoS. A comparison between measured and simulated PHS for $p = 0.87$ m (plasma centre) and 1.20 m (plasma edge) is shown in Fig. 5. The predicted neutron energy spectra are shown in Fig. 5(a): the reduction of the direct 2.45 MeV neutrons for $p = 1.20$ m is due to the peaked profile of the neutron emissivity. Measurements and simulations for different LoS with different relative back-scattered and in-scattered contributions are in good agreement as shown in Fig. 5(b): note the good agreement with the measured data even at the low energy side of the PHS where the effect of the scattered neutrons dominates. An example of the contri-
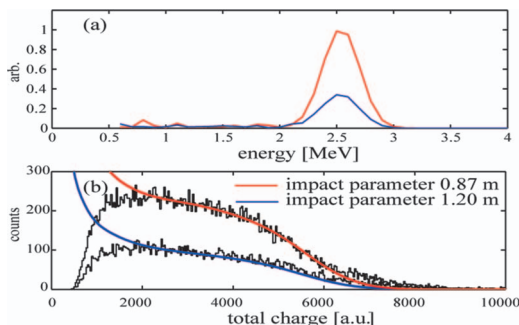

FIG. 5. (a) Calculated neutron spectrum for $p = 0.87$ m (red) and 1.20 m (blue). (b) Comparison between measured and predicted PHS.
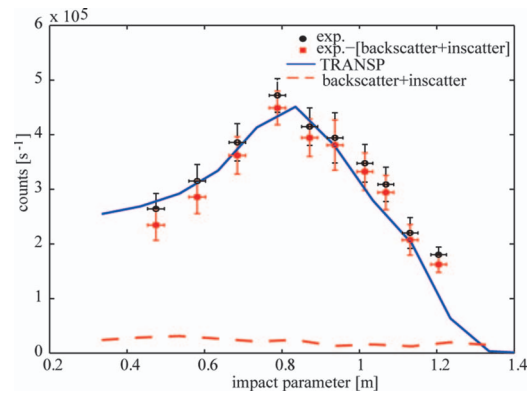

FIG. 6. Comparison between the count rates estimated by TRANSP line integrals (blue line) and the experimentally measured count rates without (black circles) and with (red squares) subtracted scattered neutron contribution.

bution of the scattered neutrons to the neutron flux profile as a function of the impact parameter is shown in Fig. 6. A series of five similar discharges (28276, 28282, 28286, 28287, and 28289) was selected for which the impact parameter p was in the range 0.5–1.2 m. During the time interval 0.26–0.28 s the plasma current is 0.8 MA, the line integrated electron density is 1.9×10^{20} m^{-2}, the NBI power is 3.2 MW. The neutron yield rate from the FC is $\approx 1.20 \times 10^{14}$ s^{-1}. The scattered neutron contribution has been estimated with MCNP for p in the range 0.3–1.3 m and it is approximately constant (dashed red line in Fig. 6). The measured neutron count rates (black circles) include the scattered neutrons reaching the detectors. The measured neutron count rates minus the scattered component (red squares) are then compared with the TRANSP simulations (solid blue line).

IV. CONCLUSIONS

The neutron energy spectrum at the detector, including the contribution of the scattered neutron, has been modelled and is in good agreement with the measured PHS. The predicted neutron energy spectra and fluxes can then be used to estimate the contribution of scattered neutrons to the experimental data for different impact parameters thus providing a better estimate of the measured neutron emissivity profiles. Good agreement is also found in this case for most impact parameters with some disagreement in the outboard region of the plasma for $p \geq 1.2$ m.

[1] M. Cecconello, M. Turnyanskiy, S. Conroy *et al.*, Rev. Sci. Instrum. **81**, 10D315 (2010).
[2] G. Dietze and H. Klein, PTB Report PTB-ND-22, 1982.
[3] S. Sangaroon, M. Cecconello, I. Wodniak *et al.*, *38th EPS Conference on Plasma Physics*, Strasbourg (2011), Vol. 35G, P5.045.